

Transit time homogenization in ischemic stroke – A novel biomarker of penumbral microvascular failure?

Thorbjørn S Engedal^{1,2}, Niels Hjort³, Kristina D Hougaard³,
Claus Z Simonsen³, Grethe Andersen³,
Irene Klærke Mikkelsen¹, Jens K Boldsen¹, Simon F Eskildsen¹,
Mikkel B Hansen¹, Hugo Angleys¹, Sune N Jespersen^{1,4},
Salvador Pedraza⁵, Tae H Cho⁶, Joaquín Serena⁵,
Susanne Siemonsen⁷, Götz Thomalla⁷,
Norbert Nighoghossian⁶, Jens Fiehler⁷, Kim Mouridsen¹
and Leif Østergaard^{1,2}

Abstract

Cerebral ischemia causes widespread capillary no-flow in animal studies. The extent of microvascular impairment in human stroke, however, is unclear. We examined how acute intra-voxel transit time characteristics and subsequent recanalization affect tissue outcome on follow-up MRI in a historic cohort of 126 acute ischemic stroke patients. Based on perfusion-weighted MRI data, we characterized voxel-wise transit times in terms of their mean transit time (MTT), standard deviation (capillary transit time heterogeneity – CTH), and the CTH:MTT ratio (relative transit time heterogeneity), which is expected to remain constant during changes in perfusion pressure in a microvasculature consisting of passive, compliant vessels. To aid data interpretation, we also developed a computational model that relates graded microvascular failure to changes in these parameters. In perfusion–diffusion mismatch tissue, prolonged mean transit time (>5 seconds) and very low cerebral blood flow (≤ 6 mL/100 mL/min) was associated with high risk of infarction, largely independent of recanalization status. In the remaining mismatch region, low relative transit time heterogeneity predicted subsequent infarction if recanalization was not achieved. Our model suggested that transit time homogenization represents capillary no-flow. Consistent with this notion, low relative transit time heterogeneity values were associated with lower cerebral blood volume. We speculate that low RTH may represent a novel biomarker of penumbral microvascular failure.

Keywords

Capillary transit time heterogeneity, ischemic stroke, magnetic resonance imaging, penumbra, perfusion

Received 4 February 2017; Revised 12 May 2017; Accepted 7 June 2017

¹Center of Functionally Integrative Neuroscience and MINDLab, Aarhus University, Aarhus University Hospital, Aarhus C, Denmark

²Department of Neuroradiology, Aarhus University Hospital, Nørrebrogade 44, 8000 Aarhus C, Denmark

³Department of Neurology Aarhus University Hospital, Aarhus C, Denmark

⁴Department of Physics and Astronomy, Aarhus University, Aarhus, Denmark

⁵Hospital Universitario Dr Josep Trueta, Girona, Spain

⁶Hospices Civils de Lyon, Lyon, France

⁷University Medical Centre Hamburg-Eppendorf, Hamburg, Germany

Corresponding author:

Thorbjørn S Engedal, CFIN – Center of Functionally Integrative Neuroscience/MINDLab, Aarhus University Hospital, Nørrebrogade 44, Building 10G, 5th floor, 8000 Aarhus C, Denmark.
Email: tsengedal@gmail.com

Introduction

Optimal management of acute ischemic stroke requires an in-depth knowledge of the hemodynamic, metabolic, and cellular events which ultimately lead to infarction. In contrast to the tremendous success of recanalization therapies in recent years,¹ the clinical impact of neuro-protective strategies remains disappointing.^{2,3} Impaired microvascular perfusion has long been suspected to affect the spatiotemporal evolution of tissue damage during an ischemic stroke.⁴ Indeed, cerebral capillaries constrict during the first hours of ischemia,^{5–7} accompanied by erythrocyte clogging,^{8,9} thrombocyte and fibrin aggregation, and formation of microthrombi.^{7,10,11} Accordingly, during ischemia, areas of capillary “no-flow” have been observed in rats,^{12–14} mice,^{7,15,16} gerbils,¹⁷ rabbits,¹⁸ non-human primates,¹⁹ and even humans.²⁰ Furthermore, experimental studies show more severe capillary no-flow with (i) more severe CBF reduction,^{13,21} (ii) prolonged duration of ischemia beyond ~1 h,^{12,21} and (iii) in the presence of baseline neurovascular impairments, including diabetes^{22,23} and hypertension.²¹ Also, in models of ischemia followed by reperfusion, some capillary no-flow persists, referred to as the *no-reflow* phenomenon.^{7,15,24}

Importantly, capillary no-flow can reduce oxygen availability in penumbral tissue in several ways. First, capillary no-flow can be so severe that blood flow is attenuated by the increase in microvascular resistance. Meanwhile, any degree of capillary no-flow causes a proportionate reduction in the capillary surface area available for oxygen exchange within the tissue.²⁵ Second, diameter reductions in perfused capillaries may be so severe that they only permit the passage of plasma,^{5,7} with only very limited content of (physically dissolved) oxygen. Meanwhile, accompanying pressure changes may cause the redistribution of capillary flows to a heterogeneous perfusion pattern with poor oxygen extraction capability, so-called ‘functional shunting’.^{26,27}

Current diagnostic approaches to assess cerebral hemodynamics in acute stroke, such as perfusion-weighted magnetic resonance imaging (PW-MRI) and computerized tomography (PW-CT), rely on the temporal dynamics of image intensity changes. These are observed in individual image voxels following the intravenous bolus injection of plasma-borne contrast agents, to arrive at parametric images of cerebral blood volume (CBV), blood flow (CBF), and their ratio, the mean transit time (MTT). Microvascular patency only affects these parameters in cases where plasma, and thereby MRI or CT contrast media, fails to reach large proportions of the microvasculature within an image voxel. Accordingly, these perfusion indices reflect blood supply and the vascular volume perfused by plasma,

but not the microvascular distribution of blood, which might reveal hemodynamic phenomena that affect the availability of oxygen in tissue. Perhaps, or as a consequence hereof, traditional hemodynamic indices have often failed to differentiate between tissue with benign oligoemia as opposed to ‘true’ penumbral tissue – that is, tissue which progress to infarction, if recanalization fails.^{28–30}

Our group has developed models to study the relation between microvascular distribution of blood flow and the extraction of oxygen, in order to quantify the effects of ‘functional shunting’.^{31–33} Recently, we have also developed methods to robustly estimate intra-voxel transit time characteristics, including their mean (MTT) and standard deviation (capillary transit time heterogeneity – CTH) by PW-MRI, and evaluated their effects on oxygen extraction efficacy in humans.^{32,34,35} Importantly, while our models and methods can relate capillary flow and flow heterogeneity to net oxygen extraction, they require that contrast media retention in brain tissue reflects capillary blood only. The dynamic images recorded as part of PW-MRI and PW-CT in acute stroke, however, are sensitive to the contrast media in all blood vessels within a voxel, whether they are small arteries, capillaries, or veins. The distribution of intra-voxel transit times derived from our methods, therefore, does not directly reflect the *capillary* distribution of plasma and erythrocytes. To fully appreciate how progressive capillary constrictions, and eventually capillary occlusions, might appear on our perfusion maps; we therefore developed a simple computational model of graded microvascular failure to aid the interpretation of our results in terms of their metabolic significance.

Both measurements and simulations show that the standard deviation of blood transit times through normal (that is, passive and compliant) anatomical microvascular networks tends to change in proportion to the mean blood transit time.^{36,37} As a consequence, CTH, our indicator of the microvascular distribution of blood, would be expected to increase in proportion to MTT in response to a reduction in perfusion pressure during an acute ischemic stroke. Such a ‘passive’ increase in CTH would therefore reflect the primary reduction in blood supply, rather than the subsequent changes in capillary patency or blood rheology across the microcirculation. To distinguish the effects of hypoperfusion and deteriorating microvascular hemodynamics, we introduced the relative heterogeneity of transit times (RTH), i.e. the CTH:MTT ratio. In statistical terms, this parameter represents the coefficient of variation. We then examined whether the acute value of these hemodynamic indices predicted subsequent infarction in a large acute stroke patient cohort. The primary outcome for our analysis of patient data

was voxel-wise risk of infarction according to 24-h recanalization status. By comparing these risk estimates with our model findings, we sought to identify microvascular biomarkers that might be of prognostic value in the management of acute ischemic stroke. Finally, we discuss these findings in terms of the putative relation between microvascular hemodynamics and metabolic derangement.

Materials and methods

Patients

Adult patients were included from the European multicenter database, *I-Know*, and a regional database, *the Aarhus Perconditioning Study*.^{38,39} In the *I-Know* database, all patients who presented within 6 h of symptom onset with acute, anterior circulation, non-lacunar, ischemic stroke with a NIHSS score ≥ 4 were included. In the Perconditioning study, all ischemic stroke patients eligible for i.v. thrombolysis treatment were included and randomized to receive treatment of four 5-min cycles of induced remote ischemia during transportation. In both studies, acute MRI was performed before i.v. thrombolysis. The *I-Know* and Aarhus pre-conditioning studies conformed with the Helsinki Declaration, the rules laid out by the Council of Europe Convention on Human rights and Biomedicine, Directive 95/46/EC of the European Parliament and of the Council of 24 October 1995 on the protection of individuals with regard to the processing of personal data and on the free movement of such data, and with the legislation and regulations in Denmark, Germany, France, and Spain, respectively. The studies were approved by the Aarhus, Hamburg, Lyon, and Girona hospitals respective regional ethics committees, and carried out after informed consent from the patients. For this study, only patients with large vessel occlusion on acute imaging and at least 20 mL of hypoperfused tissue were included (see below).

Computational model of graded microvascular failure

To 'translate' between our imaging findings on one hand, and changes in capillary patency such as those reported in the animal literature, on the other, we generated an intuitive computational model comprising of 10 capillaries of equal length organized in parallel (Figure 1). A feeding arteriole and a draining venule were placed in serial connection with the capillary network. We assumed laminar flow of a Newtonian fluid, and calculated perfusion parameters according to Hagen–Poiseuille equation. Then, assuming that oxygen exchange is limited to the capillary bed, we

calculated capillary-wise oxygen extraction according to the flow-diffusion equation²⁵ – see Figure 1 for details on parameters and formula. Based on this model, we determined the perfusion parameters one would observe, and the corresponding metabolic changes, for an image voxel in this case comprising of 23% (of the total blood volume) arterioles, 46% capillaries, and 31% venules, at baseline. Importantly, while these percentage values are close to those observed in experimental studies, the model was not designed to represent an accurate characterization of the complex cerebral microcirculation.⁴⁰ Furthermore, only relative changes to hemodynamic parameters are reported. We then emulated the effects of an ischemic stroke on the microvasculature by introducing gradual (i) reduction of perfusion pressure, (ii) capillary constriction, and (iii) capillary occlusions, in three consecutive phases.⁴¹

MRI protocol and post-processing

All patients underwent a comprehensive acute MRI protocol on admission, including diffusion-weighted imaging (DWI), T2 fluid-attenuated inversion recovery (T2-FLAIR), and perfusion-weighted imaging (PWI) using gradient echo, echo planar imaging (echo time 30–50 ms, repetition time 1500 ms, gadolinium contrast dose 0.1 mmol/kg body weight at 5 mL/s injection rate; voxel sizes 5–23 mm³). Additionally, an angiogram was obtained by *time-of-flight* imaging at admission and after 24 h. Follow-up MRI was acquired at one month, median (IQR) = 35 days (25–49), to assess final infarct based on T2-FLAIR images.^{38,42} Motion correction was performed using SPM8 (Wellcome Trust Centre for Neuroimaging, UCL, UK) running MATLAB (MathWorks Inc, Natick, MA, 2015a). Arterial input functions (AIFs) were determined semi-automatically from voxels in the territory of the contralateral middle cerebral artery.⁴³ Perfusion maps were calculated by approximating the voxel-wise transit time distribution to a gamma distribution in order to characterize the retention of tracer.³⁵ In turn, the gamma distribution is characterized solely by a shaping parameter (α) and a scaling parameter (β), and can be characterized in terms of its mean (MTT) = $\alpha \cdot \beta$, its standard deviation (CTH) = $\sqrt{\alpha} \cdot \beta$, and its coefficient of variation (RTH) = $1/\sqrt{\alpha}$. CBF was included as a parameter in the model, and thus fitted directly, while CBV was obtained as the area under the deconvolved tissue concentration curve. Values were subsequently normalized to contralateral normal appearing white matter (NAWM), defined by manual delineation of the semioval center. MTT and CTH were normalized by subtraction; CBV, CBF, and RTH by division. Normalized values of CBV and CBF were then

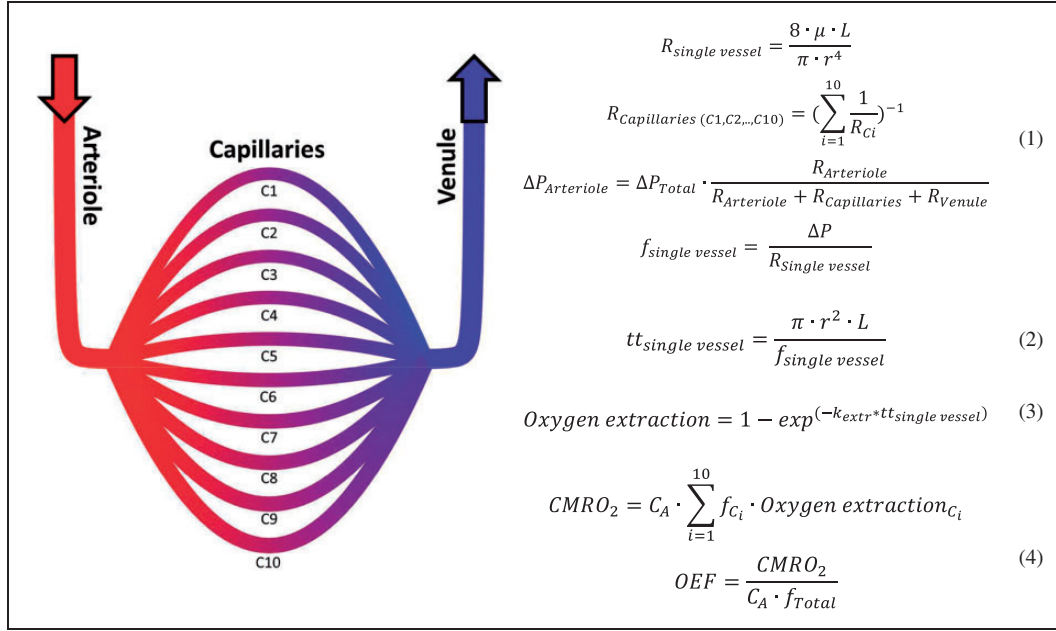


Figure 1. Computational model – design. Schematic representation of our computational model. Ten capillaries of equal length ($L = l_c$) were organized in parallel. Radii (r_c) ranged linearly between $0.08l_c$ and $0.1l_c$ at the beginning of the simulation, and between $0.065l_c$ and $0.1l_c$ after introduction of capillary constrictions. A feeding arteriole ($r_A = 0.13l_c$, $L_A = 2l_c$) and a draining venule ($r_V = 0.15l_c$, $L_V = 2l_c$) were placed in series with the capillary network. We assumed laminar flow of a non-compressible Newtonian fluid with dynamic viscosity μ , and calculated perfusion parameters according to Hagen–Poiseuilles equation (1). Here, R is resistance, r is radius, ΔP is the pressure drop over a vessel-segment, and f is flow. Then, the transit times (tt) for all vessels were calculated according to the central volume theorem (2).⁴¹ Hemodynamic parameters were calculated for the entire system (arteriole + capillaries + venule), representing the vessels found within an imaging voxel. To calculate oxygen availability, we assumed that oxygen exchange is limited to the capillary bed. Here, capillary-wise oxygen extraction was calculated according to the flow-diffusion equation (3),²⁵ where k is the exchange rate constant. We assumed that tissue oxygen tension was zero, and ignored the effects of cooperative oxygen binding.³² Having taken the effects of flow heterogeneity into account by summing over capillaries, we obtained the net oxygen extraction fraction (OEF) and the corresponding metabolic rate of oxygen ($CMRO_2$) (4), where C_A is the arterial oxygen concentration (fixed at 100%). Because hemodynamic outcomes are presented in a normalized fashion, only relative lengths matter, and l_c was thus chosen arbitrarily to be 1. The remaining variables only appear in the dimensionless combination $k\mu/\Delta P$, the value of which was set by requiring the initial total oxygen extraction fraction to be $\sim 40\%$. This was satisfied when $k\mu/\Delta P = 6.522 \cdot 10^{-5}$, realized here by setting the initial perfusion drop $\Delta P = 1$, dynamic viscosity $\mu = 1$ (in arbitrary units), and exchange rate $k = 6.522 \cdot 10^{-5} \Delta P/\mu$.

multiplied by literature reference values for healthy, normal appearing white matter,⁴⁴ while MTT, CTH, and RTH were scaled according to cohort-wise median values of normal appearing white matter (MTT = 3.2 s, CTH = 3.6 s, RTH = 1.09). Voxels with extreme values (MTT and CTH: > 100 s; CBF: > 200 mL/100 mL/min; CBV: > 100 mL/100 mL), and voxels without any bolus (CBF or CBV equal to zero) were excluded. All images were coregistered within subjects to the mean image of the acute perfusion scan using SPM8.

Region of interest

DWI lesions, if present, were manually outlined by experienced readers, who had access to apparent diffusion coefficient (ADC) and T2FLAIR images to assure that lesions represented acute diffusion restriction.

Perfusion lesions were manually outlined on time-to-peak maps to include all potentially hypoperfused voxels in the analysis. The region of interest (ROI) was then defined as the mismatch between time-to-peak and diffusion lesion masks – and referred to as *tissue-at-risk* below. Outcome was defined for each voxel according to the final infarct lesion as manually outlined on follow-up T2-FLAIR images. Perfusion and diffusion lesions were drawn by one rater. Follow-up lesions were drawn independently by four raters, and voxels accepted into the follow-up lesion if two or more raters included it.⁴⁵

Statistical analysis

Patients were grouped according to recanalization status at 24 h on the Thrombolysis in Myocardial Ischemia (TIMI) scale (TIMI ≤ 1 not recanalized,

TIMI > 1 recanalized).⁴⁶ Parametric variables were compared using the Student's *t*-test, while non-parametric variables were compared using the Mann–Whitney U test. Ratio comparison was performed using a χ^2 test. All voxel-based plots and analyses were balanced according to subject-wise voxel sizes. Perfusion variables were normalized to contralateral NAWM to allow composite voxel-wise analyses of outcome measures across all patients.⁴⁷ We performed this analysis by multiple regression, using a linear model to examine correlations and a logistic model to determine risk of infarction. To enable comparison of effect size between coefficients, perfusion variables were

furthermore standardized by subtraction of their mean and division with their standard deviation, before introduction to the models. All analyses were performed using MATLAB.

Results

Patient characteristics

A total of 126 patients met the inclusion criteria. Of these, 92 patients had recanalized after 24 h according to our imaging criteria (Table 1). Male sex and diabetes were associated with lack of recanalization, while the

Table 1. Patient demographics, stroke characteristics, and outcomes.

	Group 1	Group 2	
	24-h recanalization (<i>n</i> = 92)	No recanalization (<i>n</i> = 34)	<i>p</i> Value
<i>n</i> _{total} = 126			
Database, <i>I-Know-Stroke</i>	58 (63.0)	21 (61.8)	0.90 ^b
Demographics			
Age, years, mean (SD)	67.6 (12.6)	69.1 (11.1)	0.53 ^c
Sex, male	45 (48.9)	25 (73.5)	0.01 ^b
Weight, kg, mean (SD) ^a	74.5 (11.0)	76.6 (12.2)	0.37 ^c
Smoking, current or previous	42 (45.7)	18 (52.9)	0.47 ^b
Alcohol ^a			0.93 ^b
- No	63 (75.0)	21 (72.4)	
- ≤ 3 units/day	12 (14.3)	5 (17.2)	
- > 3 units/day	9 (10.7)	3 (10.3)	
Hypertension	62 (67.4)	26 (76.5)	0.32 ^b
Atrial fibrillation	29 (31.5)	9 (26.5)	0.58 ²
Diabetes	7 (7.6)	7 (20.6)	0.04 ^b
Stroke characteristics			
IV thrombolysis, treated ^a	73 (79.4)	27 (79.4)	0.92 ^b
Stroke type ⁴⁸			0.09 ^b
- Large vessel disease	23 (25.0)	16 (47.1)	
- Cardioembolic disease	50 (54.4)	13 (38.2)	
- Small vessel disease	1 (1.1)	1 (2.9)	
- Other or unknown etiology	18 (19.6)	4 (11.8)	
NIHSS score at admission, median (IQR)	11 (6-17)	12 (8-17)	0.22 ^d
Infarct core (DWI volume), mL, mean (SD)	21.4 (30.2)	27.2 (30.2)	0.34 ^c
Tissue-at-risk, mL, mean (SD)	120 (75.7)	109 (58.2)	0.44 ^c
Clinical and paraclinical outcomes			
NIHSS score at follow-up, median (IQR) ^a	1 (0-4)	6 (1-10)	0.006 ^d
mRS at follow-up, median (IQR) ^a	1 (0-3)	3 (1-4)	0.001 ^d
Infarct growth (in tissue-at-risk), mL, mean (SD)	12.3 (19.1)	29.6 (36.4)	0.01 ^c

Note: Values are total (%) unless stated otherwise. *P* values smaller than 0.05 are highlighted in bold. ^aMissing information (weight: *n* = 14; alcohol: *n* = 13; IV Thrombolysis *n* = 1; NIHSS at follow-up: *n* = 13; mRS at follow-up: *n* = 6).

^bChi-square test.

^cStudent's *t*-test.

^dMann–Whitney U test.

remaining demographics were similar in the two groups. Also, admission characteristics including stroke type, NIHSS score, DWI volume, and tissue-at-risk volume were similar between groups. Patients, who did not recanalize at 24 h, however, performed worse in all outcome parameters (Table 1).⁴⁸

Computational model of graded microvascular failure

Graded microvascular failure resulted in characteristic hemodynamic changes in the three phases shown in Figure 2. In Phase 1, as perfusion pressure drops, CBF decreases in a linear fashion. As a result, net oxygen availability ($CMRO_2$) also decreases. Note that oxygen extraction is inherently more efficient for longer capillary transit times, limiting the drop in $CMRO_2$. Consistent with earlier modelling results by Rasmussen et al. for passive, compliant vascular networks, no RTH changes are observed, as CTH increases in proportion to MTT.³⁷ In Phase 2, where capillary constrictions are gradually introduced across the capillary bed, both CTH and RTH increase, with a slight parallel reduction in OEF. This relation between CTH and OEF is in agreement with models in all-open capillary beds.^{32,33} Since only slight changes of capillary radii are introduced, vascular resistance only increases by ~3% (not shown), with a correspondingly small reduction of CBF. In Phase 3, as more severely affected capillaries become occluded, the observed CTH and RTH now *decrease*. This leads to increased, but largely non-nutritive, flow in the capillaries that remain open, corresponding to a reduced capillary transit time. While some ‘physiological shunting’ was introduced during Phase 2, net oxygen extraction becomes severely limited in Phase 3 as capillaries are occluded. Accordingly, $CMRO_2$ decreases at a much faster rate than CBF.

Voxel-wise investigation

MTT and CTH were highly correlated ($r^2 = 0.85$), consistent with the behaviour of a microvasculature with passive, compliant vessels.³⁷ Deviations from the ‘passive’ increase of CTH with MTT were less dependent on perfusion pressure, as indicated by the weak correlation of RTH with MTT ($r^2 = 0.21$), see Figure 3. For a given MTT value, low CTH values were associated with high risk of infarction, particularly if recanalization was not achieved – compare Figure 3(a) and 3(b). Figure 3(c) and (d) show the voxel-wise infarction rate as a function of RTH and MTT without and with recanalization, respectively. In Figure 4, two, albeit extreme, cases of persistent large vessel occlusion with markedly different outcomes illustrate the potential detrimental effects of low RTH in the absence of recanalization.

Infarct risk

In 25% of the manually delineated, perfusion-diffusion mismatch lesions, MTT values were at or below 5 s. These voxels displayed very low risk of infarction (Figure 3) and normal CBF levels (see Figure 5(b) below). These voxels were not included in the following analyses.

In tissue with prolonged MTT ($N = 852,961$ voxels; total volume = 10.8 L), the mean (standard deviation) of the perfusion variables was: MTT 13 (11) s, CTH 12 (7.6) s, RTH 1.0 (0.2), CBV 8.3 (7.2) mL/100 mL tissue, and CBF 21 (20) mL/100 mL tissue/min. In patients, who did not recanalize at 24 h, 31% of tissue with prolonged MTT infarcted vs. only 11% in patients who recanalized.

According to the central volume theorem, $MTT = CBV/CBF$.⁴¹ Including all three parameters in a logistic model might therefore make the corresponding coefficients indeterminable. The primary objective of this study was to examine the effects of RTH (and hence CTH) on infarct risk, including its interplay with both CBF and CBV. Therefore, we chose to include only RTH, CBF, and CBV in our statistical model, keeping in mind that the model was limited to voxels with prolonged MTT (>5 s). Furthermore, we allowed each predictor to affect voxel-wise survival depending on recanalization status, yielding the following formula, where R is a logical indicator of recanalization status ($R = 1$ recanalization; $R = 0$ no recanalization)

$$y = \beta_0 + \beta_1 R + \beta_2 CBF + \beta_3 CBV + \beta_4 RTH + \beta_5 CBF * R + \beta_6 CBV * R + \beta_7 RTH * R$$

Resulting coefficients for perfusion parameters, depending on recanalization status, were: no recanalization ($CBF = -0.14$, $CBV = -0.18$, $RTH = -0.62$), recanalization ($CBF = -0.61$, $CBV = -0.16$, $RTH = -0.20$). Here, coefficients in the absence of recanalization are $\beta_{2,4}$, while, in case of recanalization, the corresponding interaction with recanalization status is added ($CBF = \beta_2 + \beta_5$, $CBV = \beta_3 + \beta_6$, $RTH = \beta_4 + \beta_7$). Since all perfusion variables are normalized to their own standard deviation, coefficients can be interpreted as the expected effect, corresponding to a change of one standard deviation. Thus, for RTH, a decrease from 1.2 to 0.8 (equivalent to two standard deviations) results in a change of $-2 \cdot -0.62 = 1.24$, if recanalization is not achieved. Depending on the baseline risk, this change increases the risk of a voxel infarcting by up to 30 percentage points (according to the logistic function). Coefficients for recanalization (β_1) and the intercept of the model (β_0) were -1.22 and -1.00 , respectively. All parameters of the model were significant, except the interaction between CBV and recanalization ($p = 0.34$).

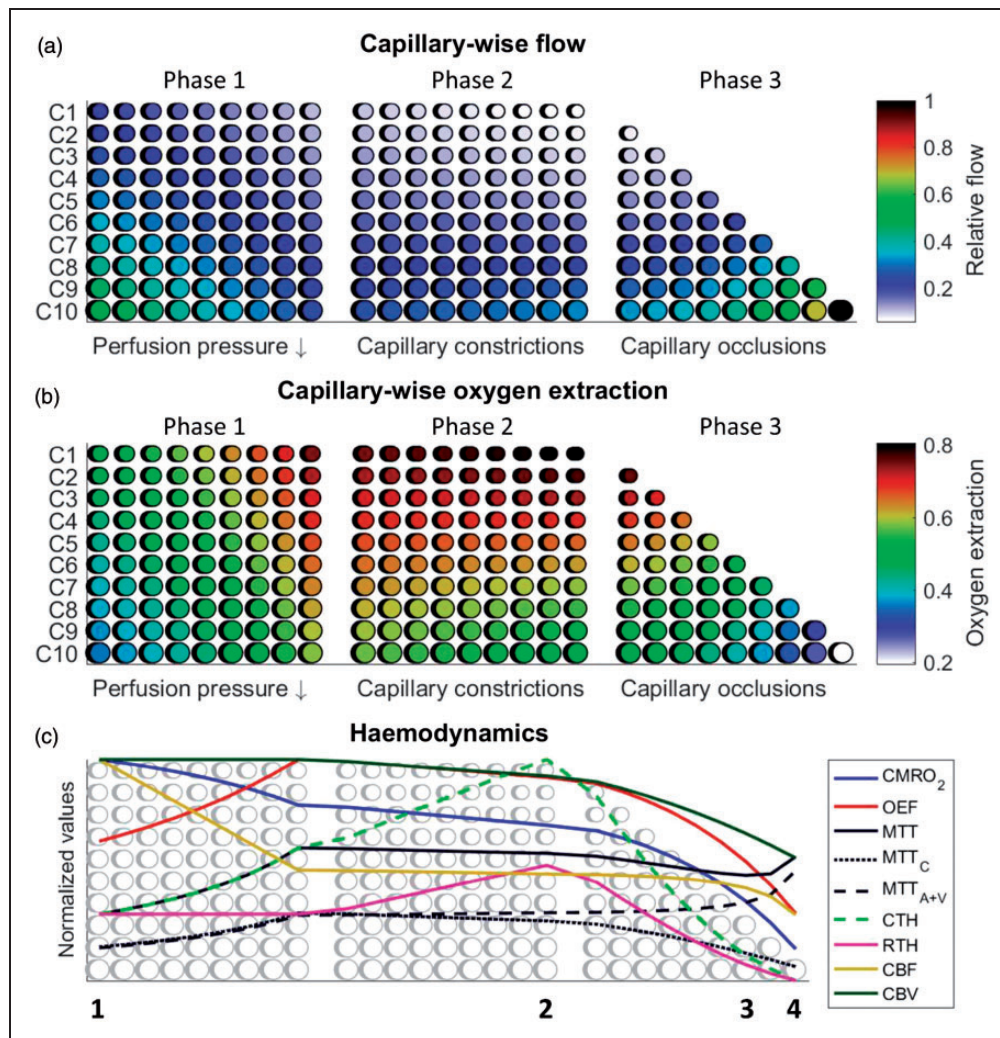


Figure 2. Computational model – resulting hemodynamic parameters. (a–c) Computational model of 10 capillaries organized in parallel and sorted according to flow. In all columns, circle sizes indicate relative vessel sizes. Size differences between individual capillaries are exaggerated to allow visual detection. Along the X-axis, we introduced hemodynamic disturbances in a graded fashion: In Phase 1 (leftmost column), we reduced the perfusion pressure to simulate the onset of a stroke (gradual, 50% reduction). Through the remaining experiment, the perfusion pressure is stationary. In Phase 2 (middle column), we constricted the smaller vessels (capillaries) to introduce more heterogeneous microscopic flows (capillary radii ranged linearly from $0.08l_c$ to $0.1l_c$ (top-to-bottom) at the beginning of phase 2, and between $0.065l_c$ and $0.1l_c$ after introduction of capillary constrictions). In Phase 3 (rightmost column), we occluded the most constricted capillaries one-by-one to simulate onset of capillary *no-flow* (Capillary occlusions). (a) Capillary-wise, normalized flow, (b) oxygen extraction for each capillary, (c) resulting hemodynamic measures. MTT, CTH, and RTH are normalized to simulate an RTH of 1 (CTH equal to MTT) at the beginning of the simulation, and relative changes of these variables are hence comparable. All other variables are normalized to their individual maximum value during the simulation. MTT represents the total transit time of the system, while MTT_C and MTT_{A+V} represent the mean transit time present in the capillary segment or the arteriolar/venular segment, respectively. Between observations 1 and 2, we reduced the perfusion pressure by 50%, while capillary constrictions lead to a 74% RTH increase. In the same interval, CBF decreased by 52%, whereas CMRO₂ only decreased by 30% (owing to prolonged capillary transit times, and thereby better oxygen extraction). Conversely, between observations 2 and 3, no changes in perfusion pressure were introduced. The step-wise onset of capillary occlusions, however, led to extreme homogenization of both CTH and RTH. Interestingly, this led to a limited CBF reduction of only 13%, whereas CMRO₂ fell by 49%. This disparity between changes in CBF and CMRO₂ is caused by a drastic reduction in OEF as blood flow is forced through the remaining open capillaries, giving rise to poor oxygen extraction efficacy. At the last observation, CMRO₂ was reduced by an additional 60%, whereas CBF only fell by 29%.

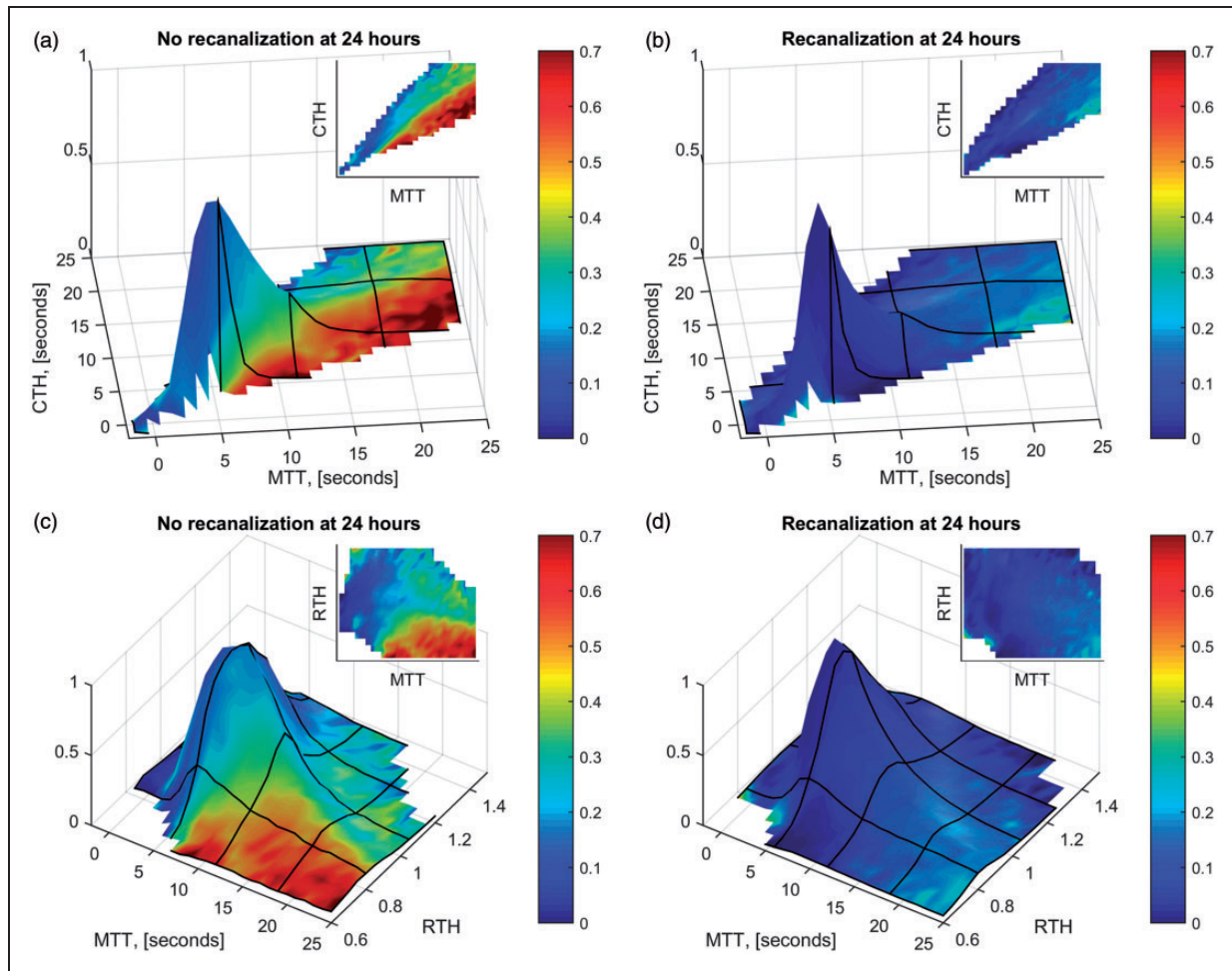


Figure 3. Voxel-wise infarction rate depending on MTT, CTH, and RTH. Plots of infarction ratios (as surface colors) as a function of MTT and CTH for mismatch tissue in which recanalization was not achieved at 24 h (Panel A) and in which recanalization was achieved (Panel B), respectively. Panels C and D show the corresponding plots as functions of MTT and RTH. The heights of the surface plots indicate the relative proportion of tissue with a given combination of these parameters. For tissue with $MTT \leq 5$ s, only a very small proportion went on to infarct at follow-up (recanalization: 7.3%; no recanalization: 14%).

Relation between RTH, CBF, and CBV

In Figure 5, mean values of CBV (panel A) and CBF (panel B) are shown according to voxels' MTT and RTH values, respectively. Note that CBV is higher in voxels with prolonged MTT, while CBF decreases steadily with increasing MTT. Also, at least for CBV, an association with RTH is readily observable. Interestingly, CBV is relatively low, although not to the level of contralateral white matter, in the region corresponding with the highest infarct risk as observed in Figure 3(c). To further investigate these observations, we devised two linear models with MTT and RTH as independent predictors of CBV and CBF, respectively. Applying the analysis to voxels with prolonged MTT (>5 s), we found significant correlations for both CBV (coefficients: MTT 1.3, RTH 1.4, $p=0$)

and CBF (coefficients: MTT -3 , RTH 3.6, $p=0$). These coefficients correspond to a CBV reduction of 1.4 mL/100 mL and a CBF reduction of 3.1 mL/100 mL/min for each 0.2 decrease in RTH, respectively.

In Figure 6, we plotted infarct risks, depending on RTH, CBV, CBF, and recanalization status. For patients, who recanalized at 24 h, CBF provided a clear, threshold-type, relationship with infarct risk at ~ 6 mL/100 mL/min. Below this threshold, the corresponding proportion of tissue that ultimately infarcted was 27% vs. only 9% in tissue with 'preserved' CBF. Corresponding proportions in patients who did not recanalize were 45% and 28%. Thus, in patients who did not recanalize, a large proportion of tissue with preserved CBF infarcted. Here, the risk of infarction was largely dependent on RTH. Thus, in decreasing quartiles of RTH, the ratio of tissue that ultimately

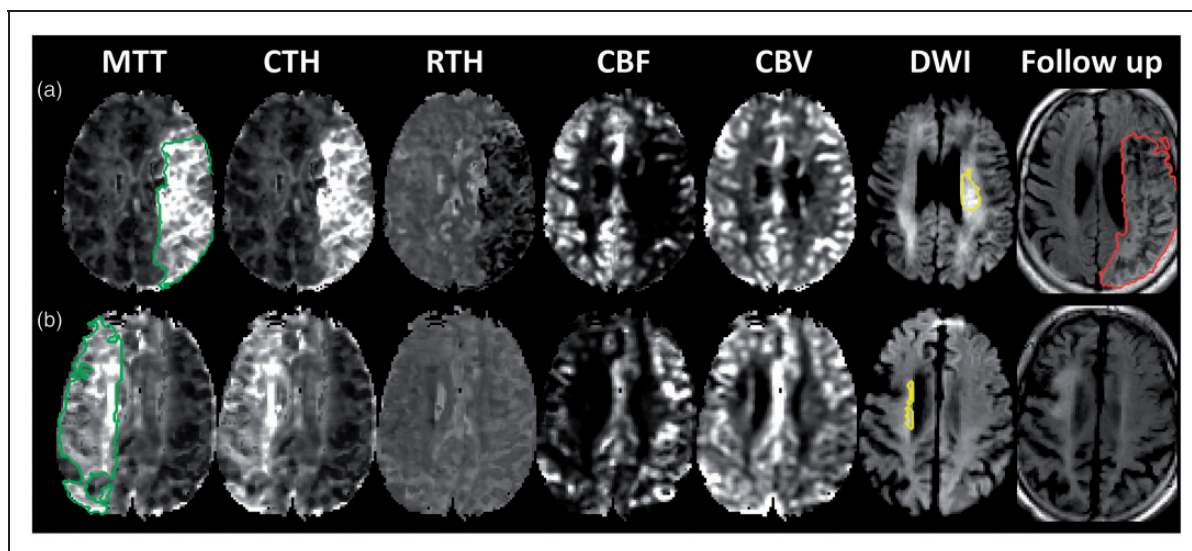


Figure 4. Patient cases. The figure shows parametric maps for two patients who presented with middle cerebral artery occlusion, none of which recanalized at 24 h. Acute perfusion lesions (green) and diffusion lesions (yellow) and follow-up T2FLAIR lesions (red) are delineated on the MTT, DWI and follow-up T2FLAIR maps, respectively. A close correlation between MTT and CTH maps is readily observed; however, the RTH maps reveal low values in the tissue at risk of patient A, whereas the RTH map is inconspicuous in patient B. Both patients present impaired CBF in the penumbra, while CBV, particularly corresponding to the cortical, leptomeningeal anastomoses, is elevated compared to the contralateral region. Conversely, CBV is low in the diffusion lesions. No infarct growth was observed in patient B, whereas the entire TTP-lesion infarcted in patient A. The dynamic range shown for the perfusion maps are: MTT and CTH 0–15 s; RTH 0.6–2; CBF 0–60 mL/100 mL/min; CBV 0–8 mL/100 mL.

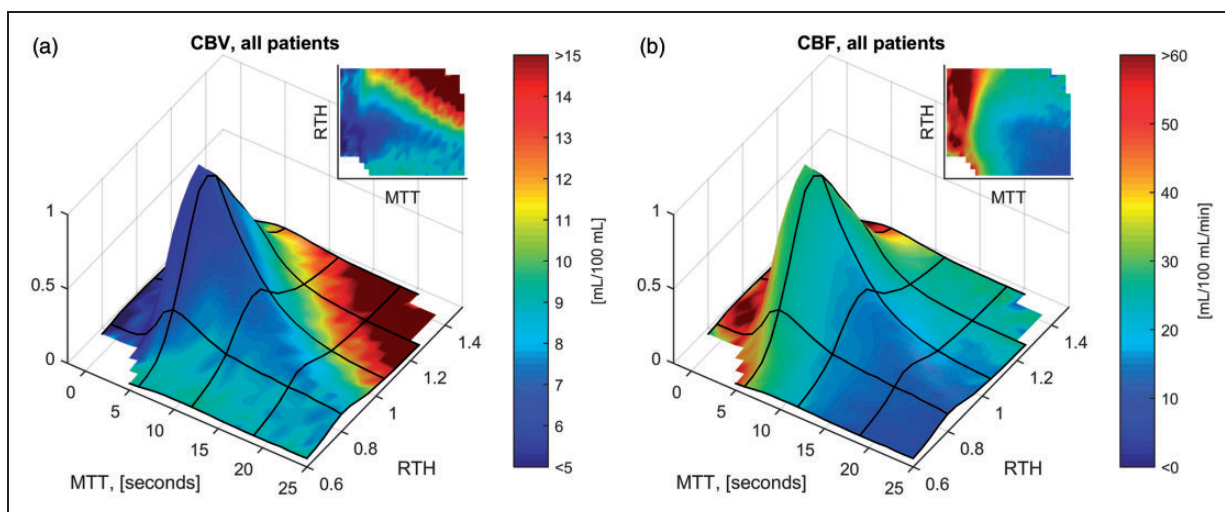


Figure 5. Relation between RTH, CBF and CBV. Surface plots of mean voxel CBV (Panel A) and CBF (Panel B), indicated as surface colors, as a function of MTT and RTH. The height of the surface plots indicate the relative proportion of tissue with a given combination of these parameters. Note that CBV is generally elevated in the tissue-at-risk, corresponding to an average value of 8.0 mL blood/100 mL, or ~ 3 times that of normal appearing white matter.⁴⁴ Additionally, mean CBV was higher in tissue with prolonged MTT (> 5 vs. ≤ 5 seconds): 8.3 vs. 6.9 mL/100 mL. Mean CBF was 43 mL/100 mL/min in tissue with MTT ≤ 5 s vs. 21 mL/100 mL/min in tissue with prolonged MTT.

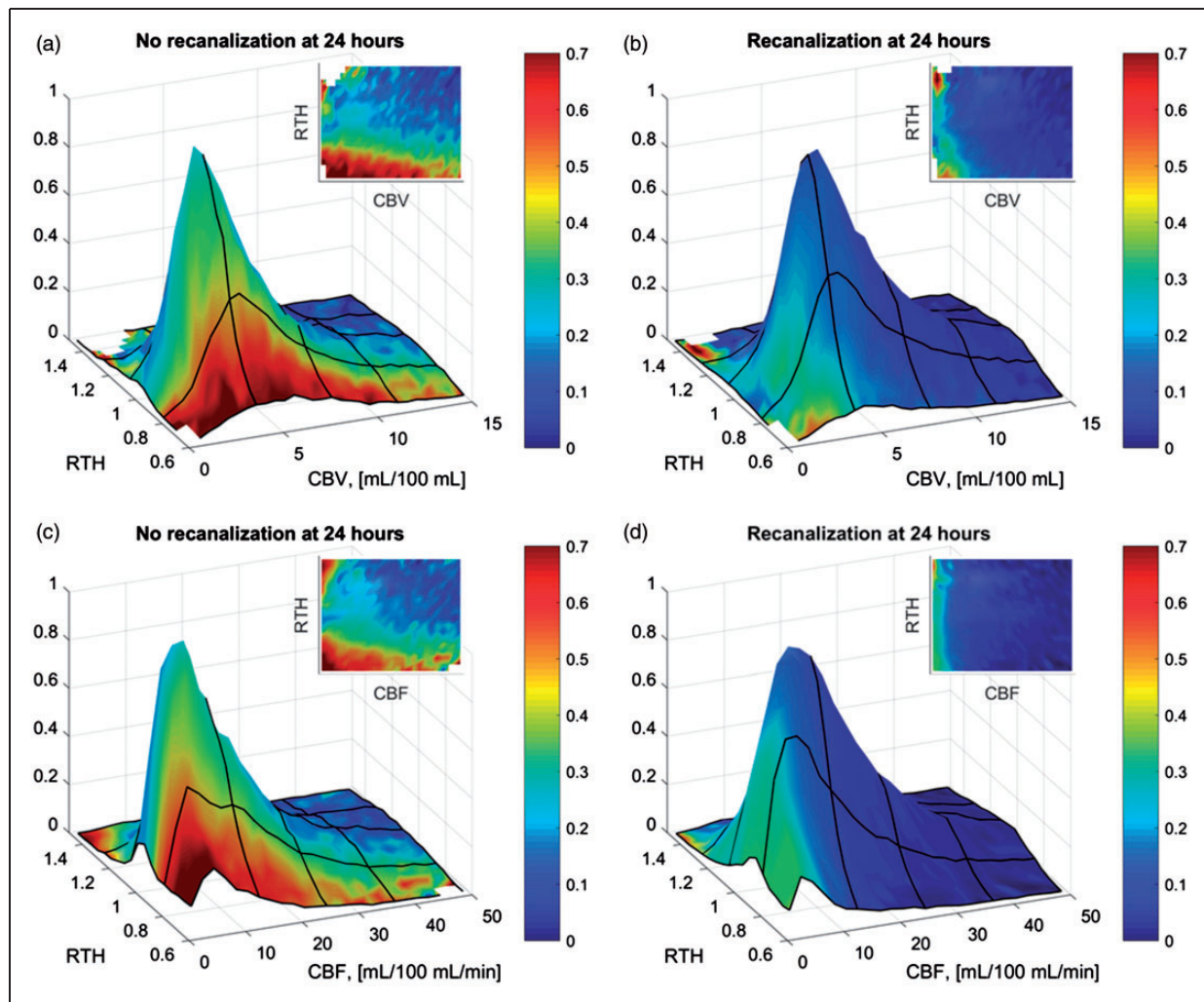


Figure 6. Voxel-wise infarction rate depending on CBV, CBF, and RTH. Plots of infarction ratios (as surface colors) as a function of CBV (a, b), CBF (c, d) and RTH for voxels with prolonged MTT (> 5 s). The heights of the surface plots indicate the relative proportion of tissue with a given combination of these parameters. For patients who recanalized at 24 h, CBF provided a clear, threshold-type, relationship with infarct risk at ~ 6 mL/100 mL/min (d). Below this threshold, the proportion of tissue that ultimately infarcted was 27% vs. only 9% in tissue with 'preserved' CBF. Conversely, in patients who did not recanalize (c), a large proportion of tissue with preserved CBF infarcted. Here, the risk of infarction was largely dependent on RTH. Thus, in decreasing quartiles of RTH the ratio of tissue that ultimately infarcted increased from 17%, through 21%, 27%, and finally 45% vs. only 7%, 9%, 10%, and 11% when recanalization was achieved.

infarcted increased from 17%, through 21%, 27%, and finally 45% vs. only 7%, 9%, 10%, and 11% when recanalization was achieved. These findings were in close agreement with the results from the logistic regression.

Time from onset analysis

The ischemic penumbra proceeds to infarction unless recanalization is achieved. This quality separates penumbral tissue from tissue with benign oligoemia. Across the entire patient population, low RTH was strongly, and almost exclusively, associated with voxel infarction

in the absence of recanalization at 24 h. Therefore, we examined whether tissue with low RTH gradually disappears as more time elapses from symptom onset. Having excluded already infarcted voxels (DWI confirmed) from our sample, we expected that hypoperfused voxels with low RTH would be more prevalent in patients who presented early vs. late. Of the 126 patients included in this study, 75 were scanned within 3 h of symptom onset, 15 after 3 h, while 36 had an uncertain onset time. Figure 1 of the Supplementary material shows the proportion of tissue, with given combinations of MTT and RTH that originated from patients scanned within 3 h

of symptom onset. Consistent with the notion that tissue with long MTT and low RTH represents penumbral tissue; such tissue was more likely to be present in patients imaged within 3 h of symptom onset, whereas voxels from patients arriving late were more likely to have normal MTT (≤ 5 s) or prolonged MTT and high RTH values.

Discussion

Herein, we present the first study to quantify and interpret microvascular perfusion heterogeneity in the human ischemic penumbra. By parametric modelling of perfusion MRI data, we characterize voxel-wise blood flow not only in terms of traditional perfusion quantities (MTT, CBF, and CBV), but also by the 'quality' of its microscopic distribution (CTH and RTH). The main finding of our study is that not only blood flow, but also its intra-voxel distribution, determines tissue fate in acute ischemic stroke. Thus, we identified regions of extreme flow homogenization as indexed by their RTH values, i.e. their relative departure from the normal relation between CTH and MTT, as particularly predictive of tissue fate. While tissue with severely restricted CBF (≤ 6 mL/100 mL/min) was likely to infarct, largely independent on recanalization status, the fate of tissue with preserved CBF (>6 mL/100 mL/min) was highly dependent on RTH. Accordingly, the proportion of tissue that infarcted increased from 17% to 44% as RTH decreased through its quartiles. Our study extends earlier human studies in which the relation between intra-voxel flow heterogeneity and tissue fate was studied using perfusion-weighted MRI.^{49–51} These studies did not quantify flow heterogeneity, but rather reported the statistical deviation of intra-voxel relative flow distributions from those observed in normal tissue. This measure provided maps that were highly correlated with final infarcts as observed on a follow up scan. Consistent with our findings, the authors reported that flow disturbances appeared to represent intra-voxel homogenizations. By using RTH as a measure of relative flow homogenization, we were able to further assert this notion, and to demonstrate that, in the absence of recanalization, RTH is a strong predictor of subsequent infarction. Indeed, tissue with prolonged MTT and low RTH seems likely to represent salvageable tissue, and our study therefore offers strong support to the notion that failing microvascular circulation is a key feature of the ischemic penumbra.^{4,7,26}

The second finding of our study is that capillary occlusions appear to play a major role in the microvascular failure identified in hypoperfused tissue. According to our computational model, step-wise occlusion of individual capillaries results in

homogenization of transit times in a simplified microvascular network. Meanwhile, in this setting, transit times in the capillaries that remain open decrease, thereby severely impairing oxygen extraction. This redistribution leads to a state of *functional shunting* with reduced oxygen availability, and thus, most likely, an increased risk of infarction. A causative link between capillary no-flow and decreasing values of CTH and RTH in the penumbra is consistent with our patient data: here, low RTH correlated with both low CBF and low CBV, while the highest risk of infarction existed, when all three variables were low, consistent with the metabolic derangement predicted by the computational model. In addition, hypoperfused, yet still non-infarcted tissue with low RTH was more likely to be present in patients who arrived early at the hospital, consistent with the gradual recruitment of penumbral tissue into the infarct core over time.

We developed a computational model to address the combined effects of functional shunting and no-flow in the microcirculation. Our previous models of tissue oxygen availability calculate the effects of functional shunting in one step, correcting for the fraction of open capillaries in a subsequent step.^{32,33} Herein, our computational model provides a convenient way of computing and visualizing the effects of graded capillary failure in a manner that captures key features of microvascular changes reported in experimental studies of ischemia, including capillary constrictions and occlusions. We note that experimental studies show augmented *no-flow* with more severe CBF reduction.^{13,21} This is consistent with our model as well as our patient data, in which we found a negative correlation between MTT and RTH, such that as MTT increased, transit time homogenization became more severe. We note that by calculating the relative heterogeneity of transit times, RTH, instead of CTH, we removed the inherent dependency of CTH on MTT.^{36,37} According to our computational model, this is particularly useful in distinguishing passive changes in the microvascular distribution of blood as a result of hypoperfusion (here, CTH increases while RTH remains constant) from physical and/or rheological changes within capillary networks that affect both CTH and RTH.

To our knowledge, three experimental studies have reported some measure of perfusion heterogeneity in models of ischemic stroke.^{14,52,53} Although all studies found some degree of increased heterogeneity, direct comparison to our results is hampered by (i) methodological differences, particularly as it pertains to perfusion measure – transit time,¹⁴ red blood cell velocity,⁵² or tracer concentration,⁵³ and lack of association with outcome. For example, Tomita et al. reported increased heterogeneity of capillary 'microflows' ($1/\text{MTT}$) after both 10 and 120 min of focal ischemia in a rat

model.¹⁴ However, paradoxically, mean microflow increased in four of five rats between 10 and 120 min of ischemia. The authors ascribed this observation to a loss of capillaries with reduced flow – i.e. onset of capillary *no-flow*. This “homogenization” did not, however, decrease the heterogeneity of microflows in the study. In the supplementary material, however, we show how this likely would have been the case, if transit times, rather than their inverse, had been used (Supplementary Figure 2).

The capillary *no-flow* phenomenon remains controversial; particularly so, as it pertains to whether capillary perfusion deficits persist after recanalization – i.e. *no-reflow*.²⁴ Our results support the notion that capillary *no-flow* is an important characteristic of the ischemic penumbra. Our results further suggest that capillary *no-flow* may be reversible with recanalization. This does not preclude that some degree of capillary *no-flow* exists in the hours following recanalization. In the Supplementary material, Figure 3, perfusion scans from a patient for which a 3-h MRI scan was available are shown. This patient presented with a middle cerebral artery occlusion, which had already recanalized at 3 h (TIMI=2), after the initial scan. Nevertheless, we observed only partial reversal of the RTH (and MTT) lesion. This is consistent with the results of Lee et al.,¹⁶ who showed persistent changes to capillary perfusion after recanalization, when the duration of the initial occlusion was extended from 1 to 2 h. Together, the observations support the notion that restoring incomplete microcirculatory reperfusion might improve outcome after an ischemic stroke.⁴ Thus, the development of therapies to ensure capillary reperfusion may therefore represent an important adjuvant to existing recanalization therapies.⁵⁴ Our results raise another intriguing question, namely whether such therapies might benefit patients who are either ineligible for recanalization therapy, or *en route* to a specialized stroke unit. Our patient data suggest that tissue with prolonged MTT, but normal RTH, has limited risk of infarction, even if recanalization is not achieved. If capillary reperfusion leads to an increase in RTH as suggested by our computational model, such therapies might therefore augment tissue survival by improving the microscopic distribution of the remaining blood supply, even if recanalization or collateral supply is incomplete.

Strengths and limitations

This study was based on two prospectively sampled databases; one applying a multi-center, observational design (I-KNOW), and the other being a single-center interventional study (Aarhus percondition study). While this approach introduces a somewhat heterogeneous study population, we took strict measures to

assure comparability between databases. Also, and of great significance, the detrimental effect of low RTH observed was consistent in sub-analyses of both databases and present independently of whether or not remote perconditioning was given (Supplementary Figure 4 and Supplementary Table 1). Interestingly, a smaller fraction of the tissue at risk infarcted in the I-KNOW database vs. the Percondition study (26% vs. 38%). This was likely explained by a longer duration between onset and acute MRI in the I-KNOW study (mean (SD): 2.8 h (1.8) vs. 1.5 h (0.4), $p=0.03$), and also reflected in larger, albeit not significantly, DWI lesions present in the I-KNOW study (mean (SD): 41 mL (38) vs. 15 mL (20), $p=0.09$). Note that the latter two analyses were confined to patients with a certain onset time ($N=90$). Importantly, both databases consisted of consecutive patients who met the inclusion criteria, and all patients were scanned immediately upon admission. We therefore believe that inclusion bias was limited in the time from onset analysis.

While our perfusion variables provided strong predictors of tissue fate, our results cannot immediately be compared to the predictive performance of other transit time metrics reported in the literature, including the commonly used T_{\max} and MTT parameters derived from nonparametric deconvolution approaches.^{55,56} These metrics are affected by, but fail to disentangle, transit time heterogeneity properties.^{34,57} In light of our findings, we speculate that this shortcoming may have affected the predictive ability of existing transit time metrics.^{28–30} Here, RTH might represent a missing step towards distinguishing tissue with benign oligoemia from salvageable tissue.

Approximation of flow patterns to the flexible two-parameter gamma function is widely used in microvascular research. Nevertheless, this approximation might not be appropriate in disease conditions such as sudden ischemia. In the Supplementary material, Figure 5, we show the residual errors after fitting gamma functions to tissue concentration time curves. Note that sum-of-squared errors are similar in normal tissue and perfusion/diffusion mismatch tissue when adjusted for CBV, which determines the local signal-to-noise ratio. This indicates that the gamma function is appropriate for both normal and hypoperfused tissue as analyzed in this study. Note that large residuals are observed in regions not reached by contrast material (cerebrospinal fluid and the diffusion lesions), as indicated by negligible CBV.

Our computational model assumes that blood flow is distributed across capillary pathways according to their respective diameters, and thus vascular resistance. Importantly, our goal was not to mimic the actual anatomical or rheological complexity of the cerebral microcirculation. Rather, the simple model design was

chosen to appreciate how changes in capillary diameter affect overall hemodynamic characteristics. In reality, erythrocyte dimensions exceed capillary diameters, and slight capillary constrictions may therefore lead to dramatic redistributions of erythrocytes and even to capillaries void of cells. The distribution of plasma in the capillary bed is less dependent on capillary diameter, as emphasized by recent experimental data.^{5,7} Accordingly, the modest reductions in CBV for low RTH may represent a dramatic reduction in the number of capillaries which carry oxygen-laden erythrocytes. When interpreting perfusion imaging data, which are based entirely on plasma flow dynamics, one might therefore only observe the “tip of the iceberg” in terms of the underlying hemodynamic and thus metabolic derangement.

Naturally, the retrospective nature of this study requires that its results should be considered hypothesis generating, and not taken as the final word on the subject matter. In particular, relating imaging findings to experimental models should be prioritized.

Conclusion

Herein, we have conducted a highly detailed analysis of the relationship between voxel-wise transit time characteristics and both traditional haemodynamic measures and ultimate risk of infarction. As an overarching conclusion, RTH proved the only parameter that distinctly separated tissue with benign oligoemia from salvageable tissue. We therefore propose that characterizations of the ischemic penumbra should be extended to include RTH, a marker of microvascular dysfunction. Furthermore, our computational model provides a rationale for the observed effect, namely, that low RTH values represent net homogenization of transit times present during widespread capillary no-flow.

Funding

The author(s) disclosed receipt of the following financial support for the research, authorship, and/or publication of this article: This study was supported by the Danish National Research Foundation (CFIN), The Danish Ministry of Science, Innovation, and Education (MINDLab), and the VELUX Foundation (ARCADIA).

Declaration of conflicting interests

The author(s) declared no potential conflicts of interest with respect to the research, authorship, and/or publication of this article.

Authors' contributions

The study was conceived by LØ. TSE and LØ designed the study. Clinical databases were collected and managed by NH, KDH, CZS, GA, IKM, SP, THC, JS, SS, GT, NN, JF, and

LØ. Methods and models were developed by MBH, HA, SNJ, KM, and LØ. Image processing was performed by TSE, MBH, SFE, JKB, and IKM. Data management and statistical analysis was performed by TSE, JKB, IKM, and KM. The computational model was developed by TSE, HA, and SNJ. TSE drafted the manuscript. All authors revised and approved the final manuscript.

Supplementary material

Supplementary material for this paper can be found at the journal website: <http://journals.sagepub.com/home/jcb>

References

1. Saver JL, Goyal M, van der Lugt A, et al. Time to treatment with endovascular thrombectomy and outcomes from ischemic stroke: a meta-analysis. *JAMA* 2016; 316: 1279–1288.
2. O'Collins VE, Macleod MR, Donnan GA, et al. 1,026 Experimental treatments in acute stroke. *Ann Neurol* 2006; 59: 467–477.
3. Minnerup J, Sutherland BA, Buchan AM, et al. Neuroprotection for stroke: current status and future perspectives. *Int J Mol Sci* 2012; 13: 11753–11772.
4. Dalkara T and Arsava EM. Can restoring incomplete microcirculatory reperfusion improve stroke outcome after thrombolysis? *J Cereb Blood Flow Metab* 2012; 32: 2091–2099.
5. Yemisci M, Gursay-Ozdemir Y, Vural A, et al. Pericyte contraction induced by oxidative-nitrative stress impairs capillary reflow despite successful opening of an occluded cerebral artery. *Nat Med* 2009; 15: 1031–1037.
6. Hall CN, Reynell C, Gesslein B, et al. Capillary pericytes regulate cerebral blood flow in health and disease. *Nature* 2014; 508: 55–60.
7. Hill RA, Tong L, Yuan P, et al. Regional blood flow in the normal and ischemic brain is controlled by arteriolar smooth muscle cell contractility and not by capillary pericytes. *Neuron* 2015; 87: 95–110.
8. Dalkara T and Alarcon-Martinez L. Cerebral microvascular pericytes and neuroglial signaling in health and disease. *Brain Res* 2015; 1623: 3–17.
9. Liu S, Connor J, Peterson S, et al. Direct visualization of trapped erythrocytes in rat brain after focal ischemia and reperfusion. *J Cereb Blood Flow Metab* 2002; 22: 1222–1230.
10. Zhang ZG, Chopp M, Goussev A, et al. Cerebral microvascular obstruction by fibrin is associated with upregulation of PAI-1 acutely after onset of focal embolic ischemia in rats. *J Neurosci* 1999; 19: 10898–10907.
11. Thomas WS, Mori E, Copeland BR, et al. Tissue factor contributes to microvascular defects after focal cerebral ischemia. *Stroke* 1993; 24: 847–853; discussion 847.
12. Garcia JH, Liu KF, Yoshida Y, et al. Brain microvessels: factors altering their patency after the occlusion of a middle cerebral artery (Wistar rat). *Am J Pathol* 1994; 145: 728–740.
13. Wang CX, Todd KG, Yang Y, et al. Patency of cerebral microvessels after focal embolic stroke in the rat. *J Cereb Blood Flow Metab* 2001; 21: 413–421.

14. Tomita Y, Tomita M, Schiszler I, et al. Moment analysis of microflow histogram in focal ischemic lesion to evaluate microvascular derangement after small pial arterial occlusion in rats. *J Cereb Blood Flow Metab* 2002; 22: 663–669.
15. Srinivasan VJ, Mandeville ET, Can A, et al. Multiparametric, longitudinal optical coherence tomography imaging reveals acute injury and chronic recovery in experimental ischemic stroke. *PLoS One* 2013; 8: e71478.
16. Lee J, Gursoy-Ozdemir Y, Fu B, et al. Optical coherence tomography imaging of capillary reperfusion after ischemic stroke. *Appl Opt* 2016; 55: 9526–9531.
17. Ennis SR, Keep RF, Schielke GP, et al. Decrease in perfusion of cerebral capillaries during incomplete ischemia and reperfusion. *J Cereb Blood Flow Metab* 1990; 10: 213–220.
18. Anderson RE, Tan WK and Meyer FB. Brain acidosis, cerebral blood flow, capillary bed density, and mitochondrial function in the ischemic penumbra. *J Stroke Cerebrovasc Dis* 1999; 8: 368–379.
19. Crowell RM and Olsson Y. Impaired microvascular filling after focal cerebral ischemia in the monkey. Modification by treatment. *Neurology* 1972; 22: 500–504.
20. Perez-Barcena J, Goedhart P, Ibanez J, et al. Direct observation of human microcirculation during decompressive craniectomy after stroke. *Crit Care Med* 2011; 39: 1126–1129.
21. Dawson DA, Ruetzler CA and Hallenbeck JM. Temporal impairment of microcirculatory perfusion following focal cerebral ischemia in the spontaneously hypertensive rat. *Brain Res* 1997; 749: 200–208.
22. Huang JY, Li LT, Wang H, et al. In vivo two-photon fluorescence microscopy reveals disturbed cerebral capillary blood flow and increased susceptibility to ischemic insults in diabetic mice. *CNS Neurosci Ther* 2014; 20: 816–822.
23. Li PA, Vogel J, Smith M, et al. Capillary patency after transient middle cerebral artery occlusion of 2 h duration. *Neurosci Lett* 1998; 253: 191–194.
24. Ames A 3rd, Wright RL, Kowada M, et al. Cerebral ischemia. II. The no-reflow phenomenon. *Am J Pathol* 1968; 52: 437–453.
25. Renkin EM. Effects of blood flow on diffusion kinetics in isolated, perfused hindlegs of cats; a double circulation hypothesis. *Am J Physiol* 1955; 183: 125–136.
26. Østergaard L, Jespersen SN, Mouridsen K, et al. The role of the cerebral capillaries in acute ischemic stroke: the extended penumbra model. *J Cereb Blood Flow Metab* 2013; 33: 635–648.
27. Kuschinsky W and Paulson OB. Capillary circulation in the brain. *Cerebrovasc Brain Metab Rev* 1992; 4: 261–286.
28. Rivers CS, Wardlaw JM, Armitage PA, et al. Do acute diffusion- and perfusion-weighted MRI lesions identify final infarct volume in ischemic stroke? *Stroke* 2006; 37: 98–104.
29. Moskowitz MA, Lo EH and Iadecola C. The science of stroke: mechanisms in search of treatments. *Neuron* 2010; 67: 181–198.
30. Sobesky J, Zaro Weber O, Lehnhardt FG, et al. Does the mismatch match the penumbra? Magnetic resonance imaging and positron emission tomography in early ischemic stroke. *Stroke* 2005; 36: 980–985.
31. Østergaard L. Principles of cerebral perfusion imaging by bolus tracking. *J Magn Reson Imag* 2005; 22: 710–717.
32. Jespersen SN and Østergaard L. The roles of cerebral blood flow, capillary transit time heterogeneity, and oxygen tension in brain oxygenation and metabolism. *J Cereb Blood Flow Metab* 2012; 32: 264–277.
33. Angleys H, Østergaard L and Jespersen SN. The effects of capillary transit time heterogeneity (CTH) on brain oxygenation. *J Cereb Blood Flow Metab* 2015; 35: 806–817.
34. Mouridsen K, Hansen MB, Østergaard L, et al. Reliable estimation of capillary transit time distributions using DSC-MRI. *J Cereb Blood Flow Metab* 2014; 34: 1511–1521.
35. Mouridsen K, Friston K, Hjort N, et al. Bayesian estimation of cerebral perfusion using a physiological model of microvasculature. *Neuroimage* 2006; 33: 570–579.
36. Duling BR and Damon DH. An examination of the measurement of flow heterogeneity in striated muscle. *Circ Res* 1987; 60: 1–13.
37. Rasmussen PM, Jespersen SN and Østergaard L. The effects of transit time heterogeneity on brain oxygenation during rest and functional activation. *J Cereb Blood Flow Metab* 2014; 35: 432–442.
38. Hougaard KD, Hjort N, Zeidler D, et al. Remote ischemic preconditioning as an adjunct therapy to thrombolysis in patients with acute ischemic stroke: a randomized trial. *Stroke* 2014; 45: 159–167.
39. Alawneh JA, Jones PS, Mikkelsen IK, et al. Infarction of ‘non-core-non-penumbra’ tissue after stroke: multivariate modelling of clinical impact. *Brain* 2011; 134: 1765–1776.
40. Weber B, Keller AL, Reichold J, et al. The microvascular system of the striate and extrastriate visual cortex of the macaque. *Cereb Cortex* 2008; 18: 2318–2330.
41. Stewart GN. Researches on the circulation time in organs and on the influences which affect it: Parts I–III. *J Physiol* 1893; 15: 1–89.
42. Carrera E, Jones PS, Alawneh JA, et al. Predicting infarction within the diffusion-weighted imaging lesion: does the mean transit time have added value? *Stroke* 2011; 42: 1602–1607.
43. Mouridsen K, Christensen S, Gyldensted L, et al. Automatic selection of arterial input function using cluster analysis. *Magn Reson Med* 2006; 55: 524–531.
44. Leenders KL, Perani D, Lammertsma AA, et al. Cerebral blood flow, blood volume and oxygen utilization. Normal values and effect of age. *Brain* 1990; 113: 27–47.
45. Hansen MB, Nagenthiraja K, Ribe LR, et al. Automated estimation of salvageable tissue: Comparison with expert readers. *J Magn Reson Imag* 2016; 43: 220–228.
46. Nighoghossian N, Hermier M, Adeleine P, et al. Baseline magnetic resonance imaging parameters and stroke outcome in patients treated by intravenous tissue plasminogen activator. *Stroke* 2003; 34: 458–463.

47. Harston GW, Tee YK, Blockley N, et al. Identifying the ischaemic penumbra using pH-weighted magnetic resonance imaging. *Brain* 2015; 138: 36–42.
48. Adams HP Jr, Bendixen BH, Kappelle LJ, et al. Classification of subtype of acute ischemic stroke. Definitions for use in a multicenter clinical trial. TOAST. Trial of Org 10172 in Acute Stroke Treatment. *Stroke* 1993; 24: 35–41.
49. Østergaard L, Sorensen AG, Chesler DA, et al. Combined diffusion-weighted and perfusion-weighted flow heterogeneity magnetic resonance imaging in acute stroke. *Stroke* 2000; 31: 1097–1103.
50. Simonsen CZ, Røhl L, Vestergaard-Poulsen P, et al. Final infarct size after acute stroke: prediction with flow heterogeneity. *Radiology* 2002; 225: 269–275.
51. Perkio J, Soinne L, Østergaard L, et al. Abnormal intra-voxel cerebral blood flow heterogeneity in human ischemic stroke determined by dynamic susceptibility contrast magnetic resonance imaging. *Stroke* 2005; 36: 44–49.
52. Hauck EF, Apostel S, Hoffmann JF, et al. Capillary flow and diameter changes during reperfusion after global cerebral ischemia studied by intravital video microscopy. *J Cereb Blood Flow Metab* 2004; 24: 383–391.
53. Vogel J, Hermes A and Kuschinsky W. Evolution of microcirculatory disturbances after permanent middle cerebral artery occlusion in rats. *J Cereb Blood Flow Metab* 1999; 19: 1322–1328.
54. Gaudin A, Yemisci M, Eroglu H, et al. Squalenoyl adenosine nanoparticles provide neuroprotection after stroke and spinal cord injury. *Nat Nanotechnol* 2014; 9: 1054–1062.
55. Albers GW, Goyal M, Jahan R, et al. Ischemic core and hypoperfusion volumes predict infarct size in SWIFT PRIME. *Ann Neurol* 2016; 79: 76–89.
56. Østergaard L, Weisskoff RM, Chesler DA, et al. High resolution measurement of cerebral blood flow using intravascular tracer bolus passages. Part I: Mathematical approach and statistical analysis. *Magn Reson Med* 1996; 36: 715–725.
57. Calamante F, Christensen S, Desmond PM, et al. The physiological significance of the time-to-maximum (T_{\max}) parameter in perfusion MRI. *Stroke* 2010; 41: 1169–1174.